Numerical Study of Inspiratory and Expiratory Flow in a Human Nasal Cavity

Vizy Nazira Riazuddin[1] Mohammed Zubair[1,*] Mohammed Zulkifly Abdullah[2]

Rushdan Ismail[3] Ibrahim Lutfi Shuaib[4] Suzina Abdul Hamid[3]

Kamarul Arifin Ahmad[1]

[1]*School of Aerospace Engineering, Universiti Sains Malaysia, Pulau Pinang 14300, Malaysia*
[2]*School of Mechanical Engineering, Universiti Sains Malaysia, Pulau Pinang 14300, Malaysia*
[3]*School of Medical Sciences, Health Campus, Universiti Sains Malaysia, Kelantan 16150, Malaysia*
[4]*Advanced Medical & Dental Institute, Universiti Sains Malaysia, Pulau Pinang, 13200, Malaysia*

Received 24 Apr 2010; Accepted 15 Sep 2010; doi: 10.5405/jmbe.781

Abstract

The complicated architecture associated with the nasal anatomy makes it difficult for visualization and measurement of flow parameters inside the nasal cavity. Objective measurement devices like rhinomanometry or acoustic rhinometry fail to assist the understanding of the physiology at every location within the nasal cavity. Therefore, in order to visualize the flow features inside the nasal cavity and to compare the inspiratory phase and expiratory phase in terms of parameters like velocity, resistance, wall shear stress, vortex formation and turbulence intensity, a computational fluid dynamics study was carried out. This study presents, the usefulness of a technique based on functional imaging and computational fluid dynamics (CFD) modeling in generating useful data that can be used to determine and diagnose upper-airway conditions. Variations in flow patterns and flow features such as pressure drop, velocity and the left and right cavity were observed. Resistance to flow was greater during inspiratory phase when compared to the expiratory phase. Turbulence intensity was more predominant during expiratory phase, whereas vortex formation could be observed only during the inspiration mechanism.

***Keywords*:** Computational fluid dynamics (CFD), Inspiration, Expiration, Resistance, Wall shear stress, Vortex

1. Introduction

Nasal airways play a very important role during respiration, not only as the gateway to the respiratory tract but also as an air conditioner regulating temperature and humidity and cleaning inspired air. The nasal cavities are two geometrically complex three-dimensional structures placed symmetrically on each side of the center of the face and separated by the nasal septum. The air entering the nostrils passes through the narrow constrict called the nasal valve and then passes through the main duct consisting of the three conchae, the superior, middle and the inferior and their underlying meatus region protruding from the lateral wall, resulting in increased resistance to the flow of air through the nasal cavity.

The complicated architecture associated with the nasal anatomy makes it difficult for the measurement of nasal resistance. Identifying the influence of nasal anatomy is made difficult by the small size of these airways and the influence of the sensitive mucosa. Several researchers have undertaken studies pertaining to airflow through nasal cavity using measuring devices such rhinomanometer and rhinoacoustic manometry [1-4]. In vivo experiments were also conducted to evaluate the flow through a cast nasal cavity [5]. There exist inherent limitations associated with these studies' objective methods and experimental investigations. Rhinomanometry cannot be used in the presence of septal perforations, and when one or both cavities are totally obstructed. Rhinomanometry is said to be affected by nasal cycle and errors as high as 25% are reported for repetitions within 15 minutes [2]. It cannot accurately assess a specific area of the nasal cavity. Rhinomanometry is time-consuming, requires a high degree of subject cooperation and is impossible in subjects with severely congested nasal airways. Acoustic rhinometry (AR) may be unreliable due to artifacts and errors can occur in cross-sectional area estimation [3]. Mean cross-sectional areas measured by AR were constantly less than those measured by

* Corresponding author: Mohammed Zubair
Tel: +6-04-5996314; Fax: +6-04-5941026
E-mail: mdzubairmanipal@gmail.com

computed tomography (CT) of the nasal cavity up to 33 mm from the nostril, whereas areas measured by AR were greater than those measured by CT scans beyond that point [6].

Even though functional imaging techniques like CT scans and magnetic resonance imaging (MRI) present visualization inside the nasal cavity, they fail to provide the essential physiological data like the effect of flow on olfactory region, vortex formation, recirculatory flow phenomenon, and many such details which are exclusively dealt with in this article. Experimental techniques such as phase Doppler interferometry can be used to determine spatial velocity profiles, however, they are time-consuming, difficult and cumbersome for conducting experiments and do not facilitate geometry modification, and are also expensive. Also, experiments can only extract resistance based on the inlet and outlet of the domain and not at any desired location inside the nasal cavity. In the event of lack of realistic measuring instruments to determine the air flow resistance as well the limitations associated with in vivo experimental measurements, the tool of computational fluid dynamics coupled with imaging data (CT or MRI) offers multifaceted benefits addressing all the issues concerned. It can be used to predict the airflow resistance when the input variables are varied. It facilitates easy modification of the geometry and allows investigations of the subject, where it would have been impossible to study using the traditional techniques. Even though a number of studies have been carried out to evaluate the flow pattern inside the nasal cavity using computational methods, a systematic study of the same, comparing the inspiratory phase with that of expiration, has not been presented [7-16]. Also the vortex formation and the role of turbinates in the flow behavior have not been specifically investigated. This CFD study allows for the investigation of the flow mechanisms in the human nasal cavity, thereby providing a platform for simulating the interaction between engineers and medical specialists, fact that can potentially yield improved diagnostic methodologies and even improved treatment strategies.

This CFD study presents flow patterns in the nasal cavity for various breathing rates. The cross-sectional variation in area between the left and right nasal cavities is determined and its effect in air flow was studied. Comparison was made between the inspiratory flow and expiratory flow. The CFD simulation adopted steady flow rates of 7.5, 10 and 15 L/min for laminar cases, whereas flow rates of 20, 30 and 40 L/min were considered turbulent. Variations in flow patterns and flow features such as pressure drop, wall shear stress, velocity and flow distribution between the left and right cavity are also presented. A comparison between the inspiratory and expiratory flow mechanisms was also studied.

2. Method

The study was based on an anatomical model of the normal nasal airway obtained from a CT scan of a healthy 39-year-old Malaysian female sourced from Universiti Sains Malaysia Medical Campus Hospital. The scan images were segmented slice by slice with an appropriate threshold value using the MIMIC (Materialise, Ann Arbor, MI) tool (Fig. 1).The 3D polyline data of the nasal cavity was then edited in CATIA (Dassault Systems, SA) and meshed with unstructured tetrahedral elements using GAMBIT 2.3 (Fluent Inc., Lebanon, PA, USA). An initial model with 106,393 cells was created and used to solve the airflow field at a flow rate of 7.5 L/min. The grid independence test resulted in an optimized grid with around 500,000 elements. The numerical simulation was performed using the commercial CFD solver FLUENT 6.3.26 (Fluent Inc., Lebanon, PA, USA). The simulation was based on the numerical solution of the Navier-Stokes equation representing the general equation for 3D flow of incompressible and viscous fluids. The SST k-ω turbulence model, a two-equation turbulence model, was employed. It was considered to be accurate and reliable with flows involving adverse pressure gradients. The suitability of the SST k-ω model had been experimentally validated by Mylavarapu et al. [8] and Ahmad et al [17].

The boundary conditions were defined based on the plug flow method cited in the literature [8-11]. The nasal wall was assumed to be rigid, and the simulation ignored the presence of mucus. A no-slip boundary condition was defined, and the inspiration mechanism was defined using mass flow inlet boundary at the nostril inlet. At the outlet, outflow boundary condition was used. Expiration was defined using mass flow boundary values at the nasopharynx with nostrils at pressure outlet boundary values. An inlet turbulence intensity of 10% was selected for the simulation. The wall y+ value was well less than 5, and the viscous effects were modeled without using any wall functions. Steady state laminar and turbulent airflow simulations were modeled. At 15 L/min, the Reynolds number obtained at the nostril inlet was around 1600, and for 20 L/min, the Reynolds number was 3100. The airflow was therefore taken to be laminar for flow rates up to 15 L/min and treated as turbulent flow beyond 15 L/min. This was also in general agreement with previous researchers, who determined the laminar nature of the flow for flow less than 15 L/min [9,23]. Simulations were carried out for flow rates of 7.5, 10, 15, 20, 30 and 40 L/min for both inspiration and expiration. Constant air density 1.217 kg/m^3 and viscosity 1.87 × 10^{-5} kg/m/s were assumed. The simulation was carried out on an IBM platform, Intel, Xenon(R) CPU, 2GB RAM, which typically took nearly 2 days of run for the complete simulation.

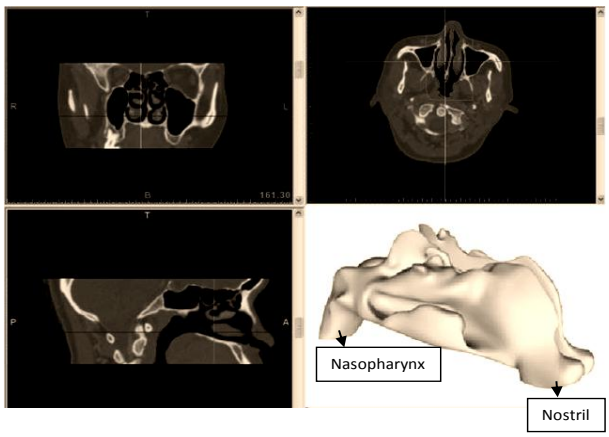

Figure 1. CT scan images and 3D polyline data of the female subject under consideration.

3. Results and discussion

3.1 Geometry comparison & model validation

The present female computational model was compared with the literature for male nasal cavities. It was observed that the cross-sectional area of the left nasal cavity was larger than that of the right nasal cavity, while in the middle region, the cross-sectional area of the left cavity was smaller than that of the right (Fig. 2). The female nasal cavity was smaller in length (8.5 cm) when compared with that of the male subjects, determined by Cheng et al and Wen et al to be 9.5 cm and 9.7 cm, respectively [9,21]. Although inter-human differences in nasal anatomy and geometry exist, the current simulation trend closely matched the established research, thereby validating the case [9,21,24]. An increase in the cross- sectional profiles was observed after the nasal valve region (Fig. 2). For the present geometry, the nasal valve region is located about 2.0 cm from the anterior tip of nose, which compares with the other models that located the nasal valve region at 3.3 cm and 2.0 cm for Cheng et al and Wen et al, respectively [9,21].

The simulation adopted laminar model for the flow rates 7.5 to15 L/min and the SST k-ω turbulent model for the flow rates 20 to 40 L/min. The average pressure drop between the nostril and nasopharynx was obtained at flow rates from 7.5 L/min to 40 L/min. The numerical results show good agreement with results obtained from other researchers, especially at flow rates less than 20 L/min. For the laminar flow rates (< 20 L/min) the slope of the impedance curve for our simulation is almost the same as found by other researchers. However, as flow rate increases, turbulence plays a significant role and the impedance curves start to depart from each other, as seen in Fig. 3 We observed that the nasal resistance in the case of female model also follows the same pattern as that of the male subjects. However, the resistance curve in the case of the female subject was much steeper than those of the male subjects seen in Fig. 3. This may be attributed the anatomical differences (the female model was shorter in length and had smaller posterior cross sectional area). The pressure drop obtained for the female nasal cavity was around 22.6 Pa for 15 L/min when compared with that of the male model, around 18 Pa and 20 Pa for the same flow rate, as obtained by Wen et al. and Weinhold et al, respectively [9,24].

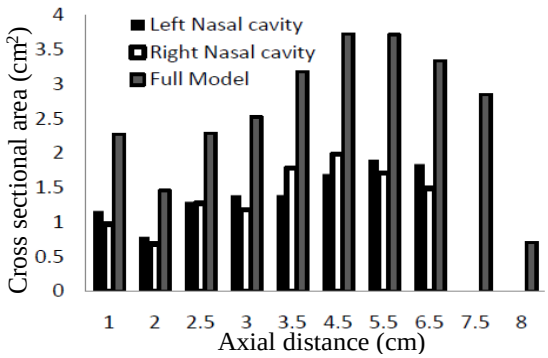

Figure 2. The comparison of cross-sectional area vs. axial distance from anterior to the posterior of the nasal cavity.

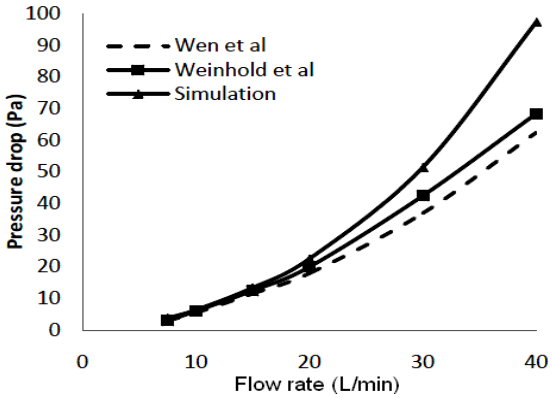

Figure 3. Pressure drop vs. inspiratory flow rates compared with previous data.

3.2 Resistance

Different resistance plots were obtained for inspiration and expiration, indicating the variation of resistance in both of the processes (Fig. 4). Lower resistance values were obtained on expiration when compared to inspiration. There is ambiguity with respect to observations on resistance during inspiration and expiration. Haight and Cole noted that during quiet respiration, the resistance to airflow was higher during inspiration when compared with expiration [18]. However, Kenyon observed the opposite and found the expiratory resistance to be higher than the inspiratory one [19]. Viani et al found the expiratory resistance to be higher when measured at a pressure gradient of 150 Pa [20]. However, the situation was reversed for low flow rates, with the inspiratory flow demonstrating lesser resistance than the expiratory one. Further studies need to be carried out to ascertain our observation. Since the present simulation study did not take into account the collapse of the nasal vestibule from the negative pressures generated during inspiration, the results obtained might not be actual physiological observations.

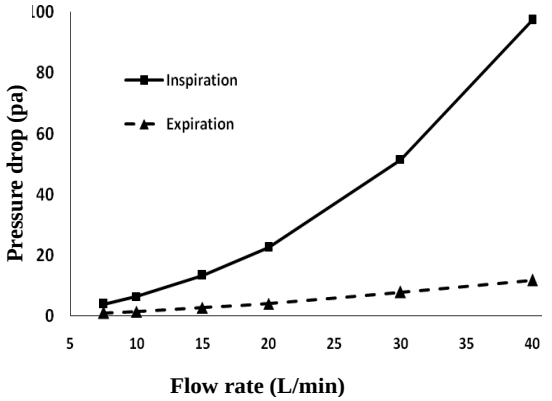

Figure 4. Resistance comparison between inspiration and expiration.

3.3 Velocity and pressure comparisons

In our model, the flow current that entered the nostril during inspiration progressed towards the nasal vestibule with a velocity of around 1.8 m/s. Figure 5 shows the variation of velocity along the length of the nasal cavity. At the narrowest cross-sectional area, also known as the nasal valve or isthmus

naris, the velocity suddenly increased to a high of around 2.4 m/s and then decreased along the middle portion where the turbinates are located. Also, the left cavity demonstrated higher velocity profiles when compared to the right cavity. It is important to determine the velocity profiles across each nasal cavity due to the asymmetric nature of the cavity. The velocity is observed to be higher at the posterior region during expiration when compared with inspiration.

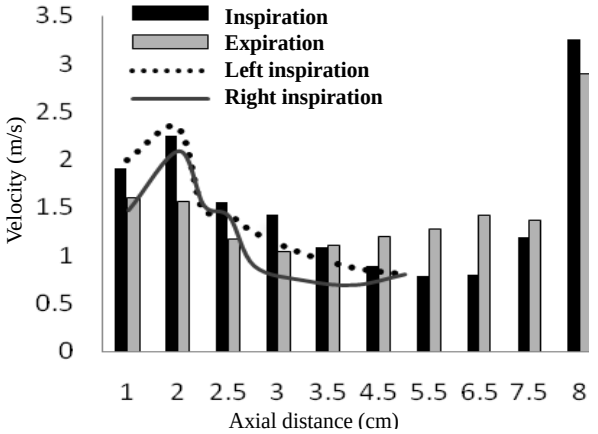

Figure 5. Velocity profile comparison during inspiration and expiration.

As observed from Fig. 6 most of the flow passed through the middle region during inspiration, whereas during exhalation, in the posterior part of the nasal cavity, much of the airflow flowed through the upper roof of the nasal cavity. The anatomical features of the nasopharynx threw the air to the top. Re-circulatory flow was observed prominently during expiration, as seen in Fig. 6B, the floor of the posterior region. The regions near the floor, roof and olfactory slit received less flow in general. It was observed that the flow that came into contact with the olfactory region was a flow recirculating at low velocity, which confirmed earlier findings [5,22,25].

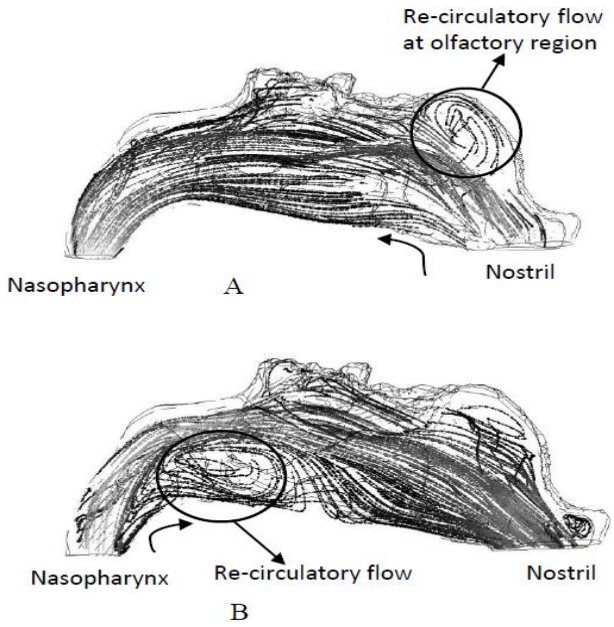

Figure 6. Pathlines during [A] inspiration and [B] expiration showing re-circulatory flow.

Pressure distribution, shown in Fig. 7, presented marked variation during inspiration and expiration. The expiratory mechanism is defined by positive pressure gradients. The flow is expelled from the lungs, and therefore there is prevalence of higher values of pressure during expiration. Whereas inspiration is the mechanism in which the lungs suck in air from the ambient atmosphere, negative pressure profile is observed for the inspiratory flow. The wall shear stresses obtained during inspiratory phase were predominantly higher in the anterior region. The maximum wall shear stress obtained at the nasal valve was around 0.97 Pa. The expiratory phase showed much higher values of wall shear stress in the posterior region (Fig. 8). In summary, the expiratory phase resulted in higher stress compared with the inspiratory phase. It can therefore be inferred that the high-velocity jet expelled during sneezing, much higher values of stress have adverse effect on the nasal wall. Continuous sneezing phenomenon may damage the nasal valve and destroy the cell lining and blood vessels attached to walls.

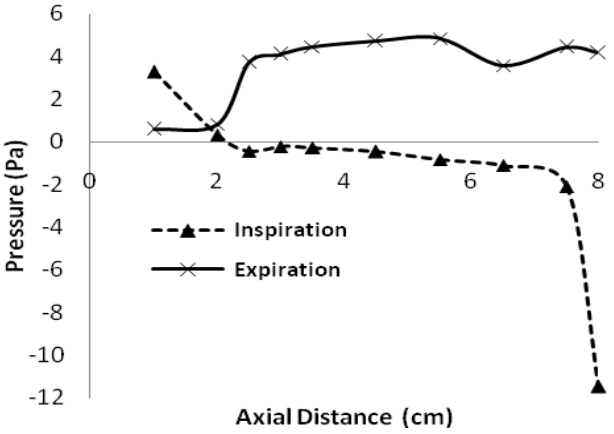

Figure 7. Average static pressure along the axial length of the nasal cavity.

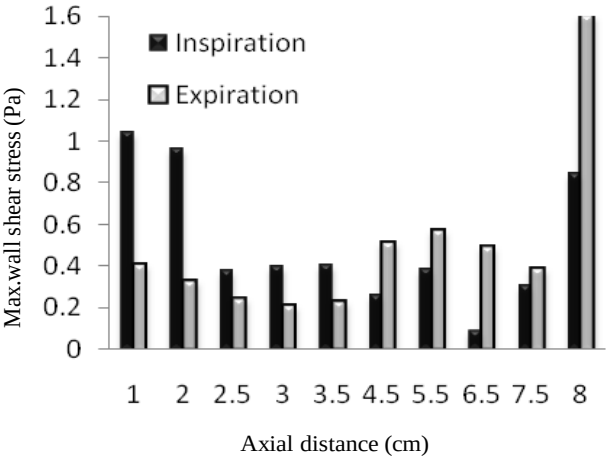

Figure 8. Maximum wall shear stress along the axial distance of the nasal cavity.

Figure 9 displays the coronal sections showing vector plots of vortex formation for flow rate of 20 L/min at locations 3.5 cm [A] and 4.5cm [B] from the tip of the nose. Inspiratory phase demonstrated vortex formation in the middle section of

the nasal cavity. The turbinates, which offer obstruction to the flow result in the formation of vortex. Conditioning of inspiratory air is one important outcome of the inspiration process. The vortex formation during inspiration results in the efficient mixing of air, and vapor from the mucous secretion also helps in exchange of heat from the blood vessels situated in the area. However, no vortex formation could be observed during the expiratory phase. The velocity vectors were normal to the flow during expiration.

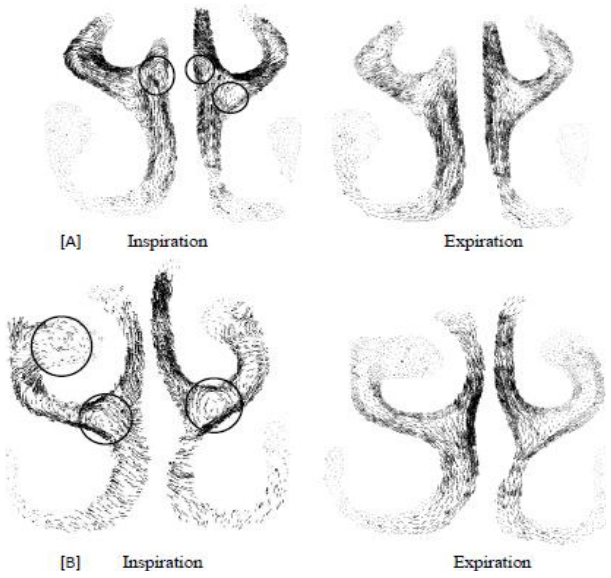

Figure 9. Coronal sections showing vector plots of vortex formation for flow rate of 20 L/min at location 3.5 cm [A] and 4.5 cm [B] from the tip of the nose. The circled areas indicate vortex formation.

Expiration phase showed higher values of turbulent intensity at the posterior regions, indicating that expiration phase demonstrates more turbulence during exhalation. Turbulence intensity plots (Fig. 10) obtained for flow rate of 20 L/min showed increased value for expiratory flow. Expiratory flow demonstrated more turbulence in the posterior region of the nasal cavity. This shows that expiratory phase is characterized by higher values of turbulence in comparison to the inspiratory phase.

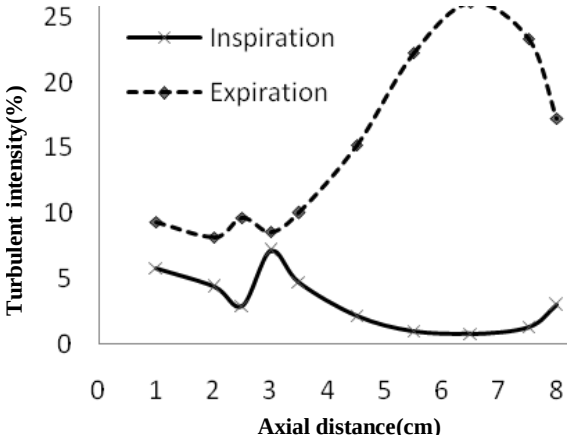

Figure 10. Turbulence intensity plot for inspiration and expiration at flow rate of 20 L/min.

4. Conclusion

In this work, the utility of the numerical model in the study of flow through the nasal cavity was shown. The model developed has been validated with the experimental results of other authors. The results of the simulation provide much more detail than the experimental findings. Also, objective measuring devices like rhinomanometry and acoustic rhinometry or the CT or MRI data fail to provide accurate measurement of details inside the cavity. Any decision made based on these measurement devices are subjected to limitations. It does not in a significant way assist the surgeon in determining the nasal resistance and understanding of flow physiology. The comparative study of the inspiratory and expiratory states has been extensively carried out, demonstrating the usefulness of numerical models in better understanding of flow phenomenon inside the nasal cavity and as such should be of benefit to medical practitioners.

Acknowledgement

The authors acknowledge the support provided through the Research University (RU) Grant No 1001/PAERO/814074 by Universiti Sains Malaysia in carrying out this work.

References

[1] K. O. Chan, Z. L. Huang and D. Y. Wang, "Acoustic rhinometric assessment of nasal obstruction after treatment with fluticasone propionate in patients with perennial rhinitis," *Auris Nasus Larynx*, 30: 379-383, 2003.

[2] O. Hilberg, A. C. Jackson, D. L. Swift and O. F. Pedersen, "Acoustic rhinometry: evaluation of the nasal cavity by acoustic rhinometry," *J. Appl. Physiol.*, 66: 295-303, 1989.

[3] A. Tomkinson and R. Eceles, "Errors arising in cross-sectional area estimation by acoustic rhinometry produced by breathing during measurement," *Rhinology*, 33: 138-140, 1995.

[4] C. E. Austin and J. C. Foreman, "Acoustic rhinometry compared with posterior rhinomanometry in the measurement of histamine and bradykinin-induced changes in nasal airway patency," *Br. J. Clin. Pharmacol.*, 37: 33-37, 1994.

[5] I. Hahn, P. W. Scherer and M. M. Mozell, "Velocity profiles measured for airflow through a large-scale model of the human nasal cavity," *J. Appl. Physiol.*, 75: 2273-2287, 1993.

[6] Y. G. Min and Y. J. Jang, "Measurements of cross-sectional area of the nasal cavity by acoustic rhinometry and CT scanning," *Laryngoscope*, 105: 757-759, 1995.

[7] K. Keyhani, P. W. Scherer and M. M. Mozell, "Numerical simulation of airflow in the human nasal cavity," *J. Biomech. Eng.*, 117: 429-441, 1995.

[8] G. Mylavarapu, S. Murugappan, M. Mihaescu, M. Kalra, S. Khosla and E. Gutmark, "Validation of computational fluid dynamics methodology used for human upper airway flow simulations," *J. Biomech.*, 42: 1553-1559, 2009.

[9] J. Wen, K. Inthavong, J. Tu and S. Wang, "Numerical simulations for detailed airflow dynamics in a human nasal cavity," *Respir. Physiol. Neurobiol.*, 161: 125-135, 2008.

[10] M. Mihaescu, S. Murugappan, M. Kalra, S. Khosla and E. Gutmark., "Large eddy simulation and Reynolds-averaged Navier-Stokes modeling of flow in a realistic pharyngeal airway model: an investigation of obstructive sleep apnea," *J. Biomech.*, 41: 2279-2288, 2008.

[11] K. Inthavong, J. Wen, Z. Tian and J. Tu, "Numerical study of fibre deposition in a human nasal cavity," *J. Aerosol. Sci.*, 39: 253-265, 2008.

[12] G. Xiong, J. Zhan, K. Zuo, J. Li, L. Rong and G. Xu, " Numerical flow simulation in the post endoscopic sinus

surgery nasal cavity," *Med. Biol. Eng. Comput.*, 46: 1161-1167, 2008.

[13] Y. Q. Huang, A. Malhotra and D. P. White, "Computational simulation of human upper airway collapse using a pressure-/state-dependent model of genioglossal muscle contraction under laminar flow conditions," *J. Appl. Physiol.*, 99: 1138-1148, 2005.

[14] V. Rakesh, A. K. Datta, N. G. Ducharme and A. P. Pease, "Simulation of turbulent airflow using a CT based upper airway model of a racehorse," *J. Biomech. Eng.*, 130: 031011, 2008.

[15] Y. Wang, Y. Liu, X. Sun, S. Yu and F. Gao, "Numerical analysis of respiratory flow patterns within human upper airway," *Acta Mech. Sin.*, 25: 737-746, 2009.

[16] C. Xu, S. H. Sin, J. M. McDonough, J. K. Udupa, A. Guez, R. Arens and D. M. Wootton, "Computational fluid dynamics modeling of the upper airway of children with obstructive sleep apnea syndrome in steady flow," *J. Biomech.*, 39: 2043-2054, 2006.

[17] K. A. Ahmad, M. Z. Abdullah and J. K. Watterson, "Numerical modeling of a pitching airfoil," *Journal Mekanikal UTM Malaysia*, 30: 37-47, 2010.

[18] J. S. J. Haight and P. Cole, "The site and function of the nasal valve," *Laryngoscope*, 93: 49-55, 1983.

[19] G. S. Kenyon, "Phase variation in nasal airway resistance as assessed by active anterior rhinomanometry," *J. Laryngol. Otol.*, 101: 910-916, 1987.

[20] L. Viani, A. S. Jones and R. Clarke, "Nasal airflow in inspiration and expiration," *J. Laryngol. Otol.*, 104: 473-476, 1990.

[21] Y. S. Cheng, H. C. Yeh, R. A. Guilmette, S. Q. Simpson, K. H. Cheng and D. L. Swift, "Nasal deposition of ultrafine particles in human volunteers and its relationship to airway geometry," *Aerosol Sci. Technol.*, 25: 274-291, 1996.

[22] R. P. Subramaniam, R. B. Richardson, K. T. Morgan, J. S. Kimbell and R. A. Guilmette, "Computational fluid dynamics simulations of inspiratory airflow in the human nose and nasopharynx," *Inhal. Toxicol.*, 10: 91-120, 1998.

[23] R. A. Segal, G. M. Kepler and J. S. Kimbell, "Effects of differences in nasal anatomy on airflow distribution: a comparison of four individuals at rest," *Ann. Biomed. Eng.*, 36: 1870-1882, 2008.

[24] I. Weinhold and G. Mlynski, "Numerical simulation of airflow in the human nose," *Eur. Arch. Otorhinolaryngol.*, 261: 452-455, 2004.

[25] M. Zubair, V. N.Riazuddin, M. Z. Abdullah, R. Ismail, I. L. Shuaib, A. H. Suzina and K. A. Ahmad, "Airflow inside the nasal cavity: visualization using computational fluid dynamics," *Asian. Biomed.* , 4: 657-661, 2010.